Molecular modelling, spectroscopic characterization and nonlinear optical analysis on N-Acetyl-DL-methionine

N. Günay[a], Ö. Tamer[b,*], D. Avcı[b], E. Tarcan[c], and Y. Atalay[b]

[a]*Beykent University, School of Health Sciences, Department of Audiology, Istanbul, Turkey.*
[b]*Sakarya University, Faculty of Arts and Sciences, Department of Physics, Sakarya, Turkey.*
[c]*Kocaeli University, Faculty of Arts and Sciences, Department of Physics, Kocaeli, Turkey.*

In this present methodical study, besed on the density functional theory (DFT), the first-principles calculations have been employed successfully to study the structural and electronic properties of *N-acetyl*-DL-methionine ($C_7H_{13}NO_3S$) which is a derivative of DL-methionine which is also known as DL-2-amino-4-methyl-thiobutanoic acid. Optimized molecular structure, vibrational frequencies, and also ^{13}C and ^{1}H NMR chemical shift values of the title compound are provided in a detailed manner by using B3LYP and HSEH1PBE functionals by applying 6-311++G(d,p) basis set for calculations using Gaussian 09W program. The comparison of the calculated values with the experimental values provides important information about the title compound. Besides the electronic properties (UV-Vis calculations) of the title compound, such as HOMO-LUMO energy values and energy gap, absorption wavelengths, oscillator strengths, were performed basing on the optimized structure in the gas phase. Moreover, the molecular electrostatic potential surface, dipole moment, nonlinear optical properties, linear polarizabilities, and first hyperpolarizabilities and chemical parameters have also been studied.

1. Introduction

Methionine is an amino acid that contains an α-amino group (protonated NH_3^+), an α-carboxylic acid group (deprotonated COO^-), and an S-methyl thioether side chain. Just like other amino acids, methionine is an organic compound used in the biosynthesis of proteins. It is also a non-polar, aliphatic amino acid and does not synthesize by the human body, so it must be obtained from foods. Methionine has the potential to the field of medicine to be used as, for example, anti-inflammatory, pain-reliever, and it stimulates the formation of cartilage tissue cells to create more cartilaginous tissue, is also used as an additive in animal feedstuffs.

All amino acids (except glycine) can exist in two isomeric forms, which are called D-(dextrorotatory) and L-(levorotatory) forms, analogous to left-handed and right-handed configurations, because of forming two different enantiomers (also called enantiomers stereoisomers and optical isomers which are mirror images to each other) around the central α-carbon atom. Methionine is one of the essential sulfur-containing amino acids, and it occurs naturally as L-methionine. A racemic DL- methionine mixture that is composed of equal amounts of D-methionine and L-methionine forms of the same compound is not optically active. Synthetic animal feed grade DL-methionine is a white crystalline powder with a faint characteristic odor and sweet, slightly bitter taste [1]. N-Acetyl DL-methionine (NAM) is one of the derivatives of DL-methionine, and, in this content, density functional theory investigations were performed on the structural, electronic, and spectroscopic properties of NAM molecule.

2. Calculation Details

In this study, the Gaussian 09W software package [2] was used to perform quantum chemical calculations, the geometry, the normal modes, HOMO-LUMO energy gaps, and the molecular electrostatic potential (MEP) surface of the title compound were visualized by GaussView 5.0 [3]. All calculations were performed in the gas phase at the DFT hybrid methods: the B3LYP (Becke's three-parameter exact exchange functional (B3) [4,5] combined with the gradient-corrected correlational functional of Lee, Yang and Parr (LYP) [6] hybrid method is also called the first-generation method) and the HSEH1PBE (it is deciphered as the Heyd, Scuseria, Ernzerhof (HSE) [7,8] hybrid combined with Perdew, Burke and Ernzerhof's exchange and correlation functions (PBE) [9], which is also known as the HSE06 approach, is a second-generation method) with 6-311++G(d,p) basis set. The selection of DFT levels can be validated by a comparison between the experimental and computed UV-Vis spectrum. The excitation energies for the title molecule calculated by B3LYP and HSEH1PBE levels in conjunction with 6-311++G(d,p) basis set were compared with the experimental emission spectrum. These levels were found to predict energies accurately, with differences between the experimental and computed excitations below the usually accepted threshold of 0.3 eV [10]. Additionally, considering that the HOMO-LUMO energy gap obtained by experimental and DFT levels are very close to each other, it will be easily understood that the selection of DFT levels is correct. The 1H and 13C NMR isotropic shielding are calcu-

lated with the GIAO (the Gauge Independent Atomic Orbital) [11-15] CSGT (the Continuous Set of Gauge Transformations) [15-17] and IGAIM (the Individual Gauges for Atoms In Molecules) [16] methods, using corresponding TMS shielding calculated at the B3LYP/6-311++G(d,p) and HSEh1PBE/6-311++G(d,p) levels. First of all, the molecular structure of TMS was optimized by the selected levels of FDT. After that, ^{1}H and ^{13}C NMR isotropic chemical shifts for TMS were computed by using GIAO, CSGT, and IGAIM method in conjunction with the same levels of DFT. The average ^{1}H and ^{13}C NMR chemical shifts for each method and DFT level were used as reference values for TMS [18,19]. The electronic properties, HOMO-LUMO energies, absorption wavelengths, and oscillator strengths are calculated using the B3LYP method of the time-dependent DFT (TD-DFT) (20-24) using the optimized parameters obtained from the B3LYP/6-311++G(d,p) method.

3. Results and discussion

3.1. Molecular Structure

In 1985, the crystal structure of NAM has been reported by Ponnuswamy and Trotter [25] and five years later, redetermined it and its calcium adduct viz., Ca(N-acetyl-DL-methionine)$_2$. H$_2$O by Kim and Eriks [26]. Moovendaran and Natarajan reported structure and some other properties by recording X-ray, IR, UV-Vis-NIR, TGA/DTA, and photoluminescence spectra [27]. According to the best of our knowledge, in the literature, there are no available spectroscopic and quantum chemical calculation results for this compound and, therefore, we calculated for the molecular structure for the first time. For the compound, we have employed a 6-311++G(d,p) basis set at B3LYP and HSEH1PBE levels without symmetry constrain, to provide integrity and compared computed geometry parameters through experimental bond lengths and bond angles, which are taken from Refs. [25,26]. The atom numbering scheme for the molecule is shown in Fig. 1a) [25].

The optimized molecular geometry of the title molecule has been obtained in the gas phase at B3LYP/6-311++G(d,p) level using is shown in Fig. 1 (b). NAM contains a carboxyl group (-C4(O2)O3H), an N-acetyl group (-NHC2O1C1H$_3$), and a side chain (-C5H$_2$SC6H$_3$C7H$_2$) attached to a C3 atom (see Fig. 1). According to the available reported studies in the literature, the calculated lattice parameters are gathered in Table I, and for these analyses confirm that the crystal belongs to the monoclinic crystal system with space group $P2_1/c$ with $Z = 4$ number of formula units in the unit cell.
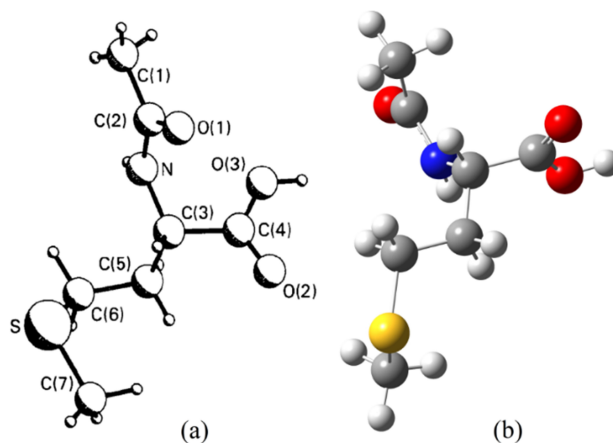
FIGURE 1. a) The experimental structure and b) the optimized molecular structure obtained by the B3LYP method for NAM.

Table II gives the unscaled theoretical geometry parameters and also experimental X-ray data of the title compound with the estimated standard deviations in parentheses. It is observed that calculated values of bond lengths and bond angles through both methods B3LYP and HSEH1PBE are closer to each other.

In consideration of the bond lengths, as shown in Table, most of the calculated values are higher than experimental ones but this can be explained by the differences in the solid-state and liquid or gas phases. The experimental values were performed for the solid phase, while the theoretical calculations were for the isolated molecule in the gas phase. The observed differences of bond parameters between the calculated and experimental values being most probably due to the subsistence of the crystal field along with the intermolecular interactions have connected the molecules, which occur in the crystal.

It can be observed that the C1-C2, C3-C4, C3-C5, and C5-C6 carbon-carbon bond lengths on the molecule are smaller than typical C-C single (1.54 Å) bond, and the C2-N bond lengths in the peptide group of the title compound are much shorter than the normal C-N single bond that is referred to 1.49 Å, which confirms this bond to have some characteristics of a double or conjugated bond [28]. The C3-N carbon-nitrogen bond length is intermediate between C-N typical single bond characteristics, as presented in related compounds previously studied [29].

C-C bond lengths in the range of $\sim 1.509 - 1.546$ Å are also close to the experimental bond lengths in the range of $\sim 1.483 - 1.531$ Å, varying with a little difference. In the

TABLE I. The unit cell parameters, angel, volume and density for NAM.

a (Å)	b (Å)	c (Å)	β (°C)	V (Å^3)	Density (g cm^{-3})	References
5.882 (1)	9.285 (1)	21.934 (3)	124.88 (5)	982.7 (2)	1.292	(25)
5.8849 (6)	9.290 (1)	18.024 (2)	92.51 (1)	984.39 (21)	1.30	(26)
5.882 (2)	9.266 (4)	18.028 (8)	92.63 (3)	-	1.29 (1)	(27)

TABLE II. Experimental and calculated bond lengths (Å), bond angles (°) and torsion angles (°) for NAM.

Parameters	Experimental	Theoretical		
Bond lengths (Å)	[25]	[26]	B3LYP	HSEH1PBE
C1-C2	1.489 (2)	1.483 (4)	1.518	1.509
C2-N	1.333 (2)	1.330 (3)	1.379	1.372
C2-O1	1.236 (2)	1.238 (3)	1.219	1.215
C3-C4	1.523 (2)	1.520 (3)	1.531	1.522
C3-C5	1.531 (2)	1.522 (3)	1.546	1.536
C3-N	1.445 (2)	1.447 (3)	1.454	1.443
C4-O2	1.207 (2)	1.205 (3)	1.204	1.201
C4-O3	1.300 (2)	1.300 (3)	1.353	1.343
C5-C6	1.518 (3)	1.526 (4)	1.530	1.522
C6-S	1.796 (2)	1.794 (3)	1.833	1.814
C7-S	1.786 (3)	1.764 (5)	1.827	1.809
Bond angles (°)				
C1-C2-N	117.2 (1)	117.5 (3)	117.5	117.2
C1-C2-O1	122.6 (1)	122.5 (2)	122.2	122.4
N-C2-O1	120.2 (1)	120.0 (2)	120.2	120.4
C4-C3-C5	108.8 (1)	110.1 (2)	109.4	109.1
C4-C3-N	112.7 (1)	112.8 (2)	112.8	113.0
C5-C3-N	110.1 (1)	108.8 (2)	111.2	111.0
C3-C4-O2	122.4 (1)	122.5 (2)	124.8	124.7
C3-C4-O3	113.4 (1)	113.3 (2)	111.9	111.9
O2-C4-O3	124.2 (1)	124.2 (2)	123.3	123.4
C3-C5-C6	114.3 (1)	114.4 (2)	112.3	112.1
C5-C6-S	115.6 (1)	115.6 (2)	114.2	114.1
C2-N-C3	121.0 (1)	121.3 (2)	128.0	127.4
C6-S-C7	101.4 (1)	102.0 (2)	100.7	100.4
Torsion Angles (°)				
O2-C4-C3-C5	-	80.3	-101.0	-99.0
O3-C4-C3-C5	-	-97.1	77.5	79.3
O2-C4-C3-N	-	-157.2	134.7	136.9
C4-C3-C5-C6	-	-172.4	167.3	168.3
C4-C3-N-C2	-	64.8	-90.6	-89.6
C5-C3-N-C2	-	-173.4	146.1	147.5
C3-N-C2-O1	-	1.9	170.1	170.0
C3-N-C2-C1	-	-177.1	-11.3	-11.4
N-C3-C4-O3 (ψ_2)	-25.5 (2)	25.4	-46.8	-44.7
N-C3-C5-C6 (χ_1)	-63.1 (2)	63.5	-67.5	-66.5
C3-C5-C6-S (χ_2)	-59.2 (2)	58.9	177.7	177.5
C5-C6-S-C7 (χ_3)	-59.3 (2)	60.4	-77.3	-75.6

title compound, the carbon sulfur bond lengths C6-S and C7-S are 1.833 Å and 1.827 Å with B3LYP and 1.814 Å and 1.809 Å with HSEH1PBE while the reported values are in the range $\sim 1.764 - 1.796$ Å [25,26]. As discussed by Johnson *et al.*, the various DFT methods predict bond lengths, which are systematically too long (30). The results of the calculated bond lengths of NAM molecule using DFT methods have provided proof of these findings. According to Table I, the computed C2-N bond length (1.379 and 1.372 Å) is a bit longer than from experimental bond lengths (1.333 and 1.330 Å).

TABLE III. Comparison of experimental and calculated vibration frequencies for NAM.

Assignments	Experimental	Theoretical			
	(27)	B3LYP		HSEH1PBE	
		Scaled freq.^{a}	I_{IR}^b	Scaled freq.^{a}	I_{IR}^b
υ(N-H)$_{as}$	3343	3435	21.2700	3469	23.5340
υ(CH$_2$)$_s$	2968	2928	24.1035	2943	22.7840
υ(CH$_2$-S)$_{as}$	2920	2919	1.1755	2936	0.7793
υ(C=O)	2461	1740	326.5540	1776	330.5009
υ(C=O)$_s$	1693	1681	495.0484	1718	515.5060
γ(N-H)	1618	1442	5.5508	1445	41.9708
β(C-N-H)	1560	1421	44.2275	1421	55.1498
υ(C-C)	1381	1297	68.8192	1303	47.8395
β(CH$_3$)	1248	1284	185.7300	1287	84.4035
τ(CH$_2$)	1190	1164	28.7162	1173	30.6745
υ(C-C-N)	1115	1082	5.3365	1099	3.8105
ρ(C-O-H)	1115	1082	5.3365	1099	3.8105
υ(C-N)	1042	1029	14.6397	1044	9.2707
υ(C-C-N)	1015	998	15.3698	961	5.4230
ρ(CH$_3$)	961	934	2.8278	936	2.9764
υ(C-C)	895	798	0.7839	812	0.4921
ρ(CH$_2$)	743	723	4.5378	723	5.5597
ω(N-H)	743	622	130.2450	623	133.9825
β(C-C)	590	567	25.7306	573	23.2463

υ: Stretching; β: in plane bending; γ: out?of plane bending; τ: twisting; ρ: rocking; ω: wagging.

^{a}Scaled frequencies are in unit of cm^{-1}.

$^b I_{IR}$ infrared inten. are in unit of km mol^{-1}.

The shortening of the bond length of C2-O1 ($\sim$1.237 Å) and C4-O2 ($\sim$1.206 Å) could be assigned a double bond character, whereas the corresponding values for the title compound are 1.219 Å 1.215 Å (B3LYP) and 1.204 Å, 1.201 Å (HSEH1PBE).

Computed C1-C2-N, C1-C2-O1, and N-C2-O1 bond lengths of the side chain have the same values (respectively, 117°, 122°, and 120°) with the experimental results. About the X-ray data, the bond angle C2-N-C3 is $\sim$ 121.2°, whereas it is computationally 128.0° and 127.4° with B3LYP and HSEH1PBE methods, respectively, which provide the possibility of the presence of hydrogen bond. According to literature [25,26] only two hydrogen bonds are formed between neighboring molecules N-H$\cdots$O2 and O3-H$\cdots$O1.

On the other hand, the carbon-carbon-oxygen bond angles in the carboxyl group lie in the range 111.9-124.8°, (DFT) and 113.3-122.5° (XRD). The bond angles are C4-C3-C5=109.3°, C4-C3-N=112.9°, and C5-C3-N=111.1°(DFT), and this asymmetry gives the interaction between the carboxyl group and the neighboring peptide group and side chain.

3.2. Vibrational wavenumbers

Vibrational frequency calculations for the ground spin state of the NAM were calculated with the same level of theory calculations based on the optimized geometries. The experimental IR spectra were compared with the calculated spectra (Fig. 2), and also theoretical and experimental absorption frequencies and assignments of the title compound are listed in Table III. The vibrational band assignments have been made using the GaussView molecular visualization program [3].

According to the literature [31], there are disagreements in the calculated harmonic vibrational frequencies when they are compared to the experimental fundamental vibrational frequencies, and these discrepancies can partially be attributed to two errors: the neglect of anharmonicity and the inaccurate description of the electron-electron interaction. A scaling factor is commonly used to correct the calculated value to match the experimental observable. Therefore, we used 0.96 [32] scale factors for the computed frequencies of the NAM. All the experimental results were confirmed by Moovendaran and Natarajan [27].
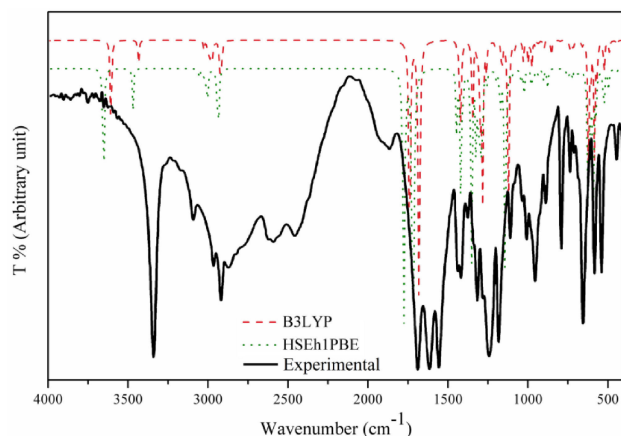
FIGURE 2. Experimental and calculated IR spectra for NAM.

The asymmetric stretching mode v(N-H) is located 3343 cm^{-1} experimentally (3435 and 3469 cm^{-1} at DFT), while the weak stretching mode v(C=O) were around 2461 cm^{-1} experimentally (1740 and 1776 cm^{-1} at DFT) after we applied the scale factor. The calculated results by frequency analysis indicate deviations from experimental values due to the intramolecular hydrogen bond between N and O. The bands corresponding to both out of the plane and in-plane C-H deformations are calculated in the region 1164-1287 cm^{-1}. The bending vibrations for γ(N-H) and β(C-N-H) groups in IR spectra are observed in the region 1618 and 1560 cm^{-1}, respectively, while the calculated vibration frequencies of them are $\sim$1444 cm^{-1} and 1421 cm^{-1}, respectively. On the other hand, the bands at 1115, 1042, and 1015 cm^{-1} are assigned to the v(C-N) vibration, and the theoretically computed values are observed in the wave region 1099-961 cm^{-1}. The theoretically computed values of ρ(CH$_3$) vibration mode at $\sim$935 cm^{-1} show a good agreement with the experimental value at 961 cm^{-1}. The IR band at 1693 cm^{-1} in the experimental IR spectrum of the title compound were designated to v(C=O) symmetric stretching fundamentals of C4 and O2 atoms, and this band appeared at 1681 cm^{-1} (B3LYP) and 1718 cm^{-1} (HSEH1PBE) in the DFT calculations. The v(CH$_2$-S) stretching mode is another typical mode for NAM, and this vibration experimentally appeared at 2920 cm^{-1}. Theoretically, this band could be assignable to: at 2919 cm^{-1} for the B3LYP method and 2936 cm^{-1} for the HSEH1PBE method.

3.3. NMR studies

The structural parameters are obtained with the B3LYP and HSEH1PBE functional and 6-311++G(d,p) basis set, and they are used to predict ^{13}C and ^{1}H NMR chemical shifts with the recommended GIAO, CSGT, and IGAIM approaches and Tetramethylsilane (TMS) is used for reference. The isotropic magnetic shielding values were used to calculate the isotropic chemical shifts (δ) with respect to TMS ($\delta_{iso}^{X} = \sigma_{iso}^{TMS} - \sigma_{iso}^{X}$). The appropriate value of the ^{1}H/^{13}C isotropic chemical shifts for TMS (σ_{iso}^{TMS}) was found to be 184.0807/31.9723 ppm for GIAO, 182.3844/30.7302

ppm for IGAIM, and 182.3611/30.7287 ppm for CSGT by B3LYP/6-311++G(d,p). Those obtained by HSEH1PBE level were also found to be 188.3372/31.8158ppm for GIAO, 186.7863/30.5605 ppm for IGAIM, and 186.7641/30.5590 ppm for CSGT.

The experimental and theoretical values for ^{13}C and ^{1}H NMR chemical shifts of the title molecule are given in Table IV. The correlation values between the experimental and calculated chemical shifts in Table IV shows that all computations are in good agreement with the experimental data except the proton of the amino group in ^{1}H NMR. The chemical shifts of the hydrogen atoms of the CH$_3$ groups are 2.040 ppm (C1), 1.850 ppm (C7), and the hydrogen atom of the CH$_2$ groups are 1.93 (C5), 1.82 ppm (C5), 2.48 ppm (C6) experimentally. In our present investigation, the chemical shifts of hydrogen atoms in the CH$_3$ groups are calculated in the range 1.036- 2.270 ppm, and in the CH$_2$ groups are in the range 1.324 - 2.713 ppm. The chemical shift value of the H atom bonded to C3 is calculated in the range 3.668 - 2.949 ppm and observed at 4.284 ppm.

There are seven carbon atoms in the title molecule, and the ^{13}C NMR spectrum of the NAM exhibits seven signals. The signal at 173.36 ppm is assigned to the C4 carbon atom of the carboxyl group computed as in the range 178.167 - 173.800 ppm. As would be expected, ^{13}C NMR chemical shifts for C4 and C2 atoms are calculated as higher than the other C atoms due to the electronegativity properties of O and N atoms. As can be seen from Table IV, the theoretical ^{13}C chemical shift results for NAM are generally closer to the experimental ^{13}C shift data.

3.4. Non-linear optical (NLO) analysis

The electric dipole (hyper) polarizabilities of a molecule are a measure of the ability to respond to an electric field (E) [33] and determine the strength of molecular interactions (long-range intermolecular induction and dispersion forces), the cross sections of different scattering, collision processes [34] and the nonlinear optical properties of the system [35].

In the presence of the electric field, the expectation value of the electric dipole moment is the sum of a permanent dipole moment and the contribution induced by the field:

$$\langle \mu \rangle = \mu_0 + \alpha E + \frac{1}{2}\beta E^2 + \cdots \tag{1}$$

In this expression, α is the linear polarizability, and β is the first hyperpolarizability (else, sometimes, second-order or quadratic hyperpolarizability).

The relation between the three Cartesian components of the dipole moment vector ($\vec{\mu}$) and the three Cartesian components of the electric field vector ($\vec{E}$) requires nine proportionality factors, therefore α is a second rank tensor that can be described by a 3×3 matrix with the 9 components. The second interaction involves evaluating the effect on the dipole moment of combinations of Cartesian components of the field; therefore, β is the third rank tensor that can be de-

TABLE IV. Experimental and theoretical ^{13}C and ^{1}H isotropic chemical shifts for NAM.

Atom	Experimental	Theoretical					
		GIAO		IGAIM		CSGT	
^{13}C		B3LYP	HSEH1PBE	B3LYP	HSEH1PBE	B3LYP	HSEH1PBE
C4	173.36	178.167	176.345	175.443	173.832	175.411	173.800
C2	169.38	174.759	172.713	172.615	170.775	172.589	170.749
C3	50.86	63.419	60.409	61.876	58.939	61.852	58.915
C6	30.65	39.776	36.948	39.541	36.708	39.527	36.694
C5	29.63	39.296	36.922	38.774	36.526	38.761	36.512
C1	22.26	22.431	22.061	20.300	19.889	20.297	19.885
C7	14.46	21.013	19.251	21.147	19.419	21.148	19.419
R^2		0.9968	0.9980	0.9960	0.9974	0.9960	0.9974
^{1}H							
H (O3)	-	5.641	5.557	4.739	4.659	4.741	4.661
H (N)	8.16	4.587	4.502	4.055	3.979	4.047	3.971
H (C3)	4.284	3.688	3.701	2.962	2.998	2.949	2.985
H (C6)	2.48	2.713	2.707	2.300	2.278	2.292	2.269
H (C6)	2.48	2.356	2.309	1.645	1.605	1.639	1.599
H (C7)	1.850	2.270	2.230	1.919	1.862	1.919	1.861
H (C7)	1.850	1.973	1.888	1.639	1.537	1.639	1.537
H (C1)	2.040	1.881	1.841	1.203	1.168	1.198	1.163
H (C7)	1.850	1.853	1.858	1.270	1.240	1.271	1.242
H (C1)	2.040	1.852	1.826	1.119	1.091	1.115	1.087
H (C1)	2.040	1.851	1.835	1.065	1.039	1.062	1.036
H (C5)	1.93	1.829	1.807	1.392	1.379	1.384	1.370
H (C5)	1.82	1.809	1.780	1.353	1.331	1.345	1.324
R^2		0.8924	0.8807	0.8445	0.8396	0.8445	0.8400

scribed by a $3 \times 3 \times 3$ matrix with the 27 components. According to Kleinman symmetry, α can be reduced into 6 components ($\alpha_{xy} = \alpha_{yx}$, $\alpha_{xz} = \alpha_{zx}$, $\alpha_{zy} = \alpha_{yz}$) and β can be reduced into 10 components ($\beta_{xyy} = \beta_{yxy} = \beta_{yyx} = \beta_{yyz} = \beta_{yzy} = \beta_{zyy}...$) [36]. In the lower tetrahedral point group, the Gaussian 09W output file printout of the α matrix is α_{xx}, α_{xy}, α_{yy}, α_{xz}, α_{yz}, α_{zz}, and β matrix is β_{xxx}, β_{xxy}, β_{xyy}, β_{yyy}, β_{xxz}, β_{xyz}, β_{yyz}, β_{xzz}, β_{yzz}, β_{zzz}.

For the title molecule, we use the following expressions to calculate. The dipole moment,

$$\mu = \sqrt{\mu_x^2 + \mu_y^2 + \mu_z^2}. \tag{2}$$

The isotropic polarizability,

$$\langle \alpha \rangle = \frac{1}{3}(\alpha_{xx} + \alpha_{yy} + \alpha_{zz}). \tag{3}$$

The anisotropy polarizability,

$$\Delta\alpha = \left\{ \frac{1}{2}\left[(\alpha_{xx} + \alpha_{yy})^2 + (\alpha_{yy} + \alpha_{zz})^2 \right. \right.$$
$$\left. \left. + (\alpha_{zz} + \alpha_{xx})^2 + 6\left(\alpha_{xy}^2 + \alpha_{xz}^2 + \alpha_{yz}^2 \right) \right] \right\}^{1/2} \tag{4}$$

And the magnitude of the first order hyperpolarizability tensor ($\langle \beta \rangle$) is defined in terms of three axes as:

$$\langle \beta \rangle = \left[(\beta_x)^2 + (\beta_y)^2 + (\beta_z)^2 \right]^{1/2} \tag{5}$$

where, in general, components equation of β can be calculated using the following equation:

$$\beta_i = \beta_{iii} + \frac{1}{3}\left[\sum_{i \neq j} \beta_{ijj}^2 + \beta_{jij}^2 + \beta_{jji}^2 \right]^{1/2} \tag{6}$$

The complete equation for the β in terms of Cartesian components leads to:

$$\langle \beta \rangle = \left[\left(\beta_{xxx} + \beta_{xyy} + \beta_{xzz} \right)^2 + \left(\beta_{yyy} + \beta_{xxy} + \beta_{yzz} \right)^2 \right.$$
$$\left. + \left(\beta_{zzz} + \beta_{xxz} + \beta_{yyz} \right)^2 \right]^{1/2} \tag{7}$$

In this study at DFT with 6-311++G(d,p) basis set, based on the finite field (FF) approach, parameters such as the total

TABLE V. Total static dipole moment (μ), the mean polarizability ($\langle\alpha\rangle$), the anisotropy of the polarizability ($\Delta\alpha$) and the mean first-order hyperpolarizability ($\langle\beta\rangle$) for NAM (units in esu).

Property	B3LYP	HSEH1PBE	pNA	Urea
μ_x	-1.184	-1.101		
μ_y	1.601	1.637		
μ_z	0.314	0.414		
$\mu/$ Debye	2.016	2.015	6.2 [40]	4.56 [41]
α_{xx}	20.5	20.1		
α_{yy}	17.6	17.2		
α_{zz}	17.1	16.8		
$\langle\alpha\rangle/10^{-24}$	18.4	18.1	17.0 [40]	
$\Delta\alpha/10^{-24}$	3.15	3.10		
β_x	1.58	1.64		
β_y	1.33	1.15		
β_z	-0.69	-0.62		
$\langle\beta\rangle/10^{-30}$	2.17	2.10	16.9 [42,43]	

static dipole moment (μ), the component of the dipole moment ($\mu_i(i = x, y, z)$), the isotropic polarizability ($\langle\alpha\rangle$), the anisotropy of the polarizability ($\Delta\alpha$), the first order hyperpolarizability ($\langle\beta\rangle$) are calculated by using B3LYP and HSEH1PBE functionals for NAM and collected in Table V. Also, Table V collects these parameters for two reference molecules, *i.e.*, urea and para-nitroaniline (pNA). Urea and pNA are well-known prototypical donor-acceptor organic standards with large hyperpolarizability [37-42]. The first-order hyperpolarizability values for NAM are higher than urea and pNA molecules.

All the tensors values of the Gaussian 09W program output file are reported in the atomic system of the unit (a.u.) and therefore the calculated values are converted into electrostatic units (esu) (for $\langle\alpha\rangle$ and $\Delta\alpha$ 1 a.u. $= 0.1482 \times 10^{-24}$ esu and for $\langle\beta\rangle$ 1 a.u. $= 8.6393 \times 10^{-33}$ esu).

3.5. HOMO-LUMO gap (HLG) analysis

The terms HOMO and LUMO are shorthand for the highest occupied and lowest unoccupied molecular orbitals, respectively. HOMO is the orbital of the highest energy for a molecule that contains electrons, and the empty molecular orbital that is closet in energy to the HOMO is called the LUMO. The HOMO and LUMO are the frontier orbitals: the frontier is the site of much of the reactive and spectroscopic activity of the species.

The DFT calculations that are the main working horse for ground-state properties such as atomic structures and binding energies significantly underestimate band gaps in particular the Kohn-Sham eigen energy. In prior studies, band structures predicted by the DFT method are reported to match experimental observations [43].

Ionization energy is the energy required to remove an electron from a neutral atom. The first ionization energy can also be defined as the energy to remove one electron from a neutral atom, to make an ion with a positive charge. Electron affinity is to do with the energy required to add an electron to a neutral atom to become a negative ion. To evaluate the relative reducibility of the title compound, ionization potential and electron affinity were calculated from differences of total energies of the neutral (E_{NEUTRAL}) and ionic systems (E_{CATION}, E_{ANION}) obtained from optimized molecular configurations using the following equations.

The ionization potential,

$$IP = E_{\text{CATION}} - E_{\text{ANION}}. \tag{8}$$

The electron affinity,

$$EA = E_{\text{NEUTRAL}} - E_{\text{ANION}}. \tag{9}$$

The restricted calculation was used in computing the total energy for the neutral ground state, whereas the unrestricted model was used for cations and anions.

According to Koopmans' theorem, the first ionization energy directly relates to removing an electron from the orbital is given by the negative value of the energy of the orbital ($IP = -E_{\text{HOMO}}$) if the wave function relaxations are ignored, as calculated within the Hartree-Fock theorem [44]. In the literature, this theorem has become generally accepted.

Based on the HOMO and LUMO energy for the title molecule, we use the following expressions to calculate.

The electronegativity:

$$\chi = (IP + EA)/2. \tag{10}$$

The chemical potential:

$$\mu = -\chi = -(IP - EA)/2, \tag{11}$$

[45].

TABLE VI. Frontier orbital energies and calculated physico-chemical properties for NAM.

Property		B3LYP	HSEH1PBE
HOMO energy	E_{HOMO} (eV)	-6.364	-6.180
LUMO energy	E_{LUMO} (eV)	-0.899	-1.006
HOMO-LUMO energy gap	ΔE (eV)	5.464	5.174
Ionization potential	IP (eV)	8.405	8.389
Electron affinity	EA (eV)	-0.225	-0.255
Electronegativity	χ (eV)	4.090	4.067
Chemical potential	μ (eV)	-4.090	-4.067
Global hardness	η (eV)	4.315	4.322
Global softness	S (eV^{-1})	0.232	0.231
Electrophilicity	ω (eV)	1.938	1.913

HOMO–1 (50)   HOMO (51)   LUMO (52)   LUMO +1 (53)
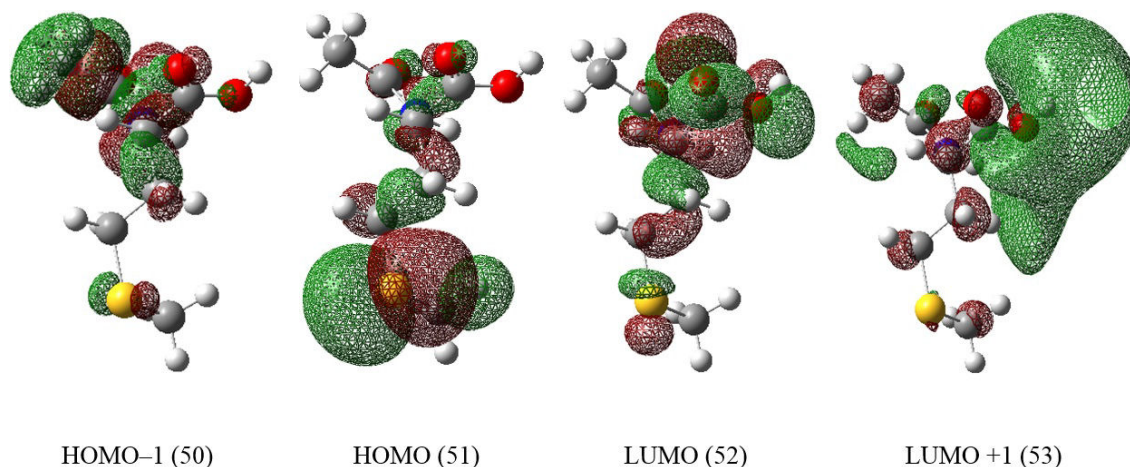
FIGURE 3. The FMOs, energies (in eV), and HOMO-LUMO energy gaps of NAM calculated at B3LYP.

The hardness:

$$\eta = (IP - EA)/2 \qquad (12)$$

[46-48].

The softness:

$$S = 1/\eta. \qquad (13)$$

The electrophilicity (in terms of chemical potential and hardness):

$$\omega = \mu^2/2\eta. \qquad (14)$$

The single point energies and frontier molecular orbitals (FMOs) were determined according to quantum chemical calculations, and in these calculations, molecular orbital 51 (the HOMO) is described by as much as 363 molecular orbital coefficients, each of the thirteen hydrogen atoms contributing 7, the three oxygen, seven carbon, and nitrogen atoms contributing 22 and sulfur contributing 30 basis functions. The quantum chemical parameters of the molecule are summarized in Table VI.

The HOMO which is the outermost orbital containing electrons and its vicinal orbital, play an important role in electron donor, while the LUMO, which is the innermost orbital containing free places to accept electrons and its vicinal orbital, play an important role in electron acceptor. The energy value of HOMO was computed as -6.364 eV (B3LYP), -6.180 eV (HSEH1PBE) and LUMO as -0.899 eV (B3LYP), -1.006 eV (HSEH1PBE). The HOMO-LUMO energy gap, which reflects optical and electric properties and chemical activity of the molecule was calculated 5.464 eV (B3LYP) and 5.174 eV (HSEH1PBE); both the values were strongly supported the previous work (5.2 eV [27]). To understand the bonding scheme and facilitate discussion of the transitions of the title compound, contour plots of FMOs, HOMO-1 to LUMO+1, are presented in Fig. 3 for the molecule in the gas phase. The red and green colors of the molecular orbital's plot show the
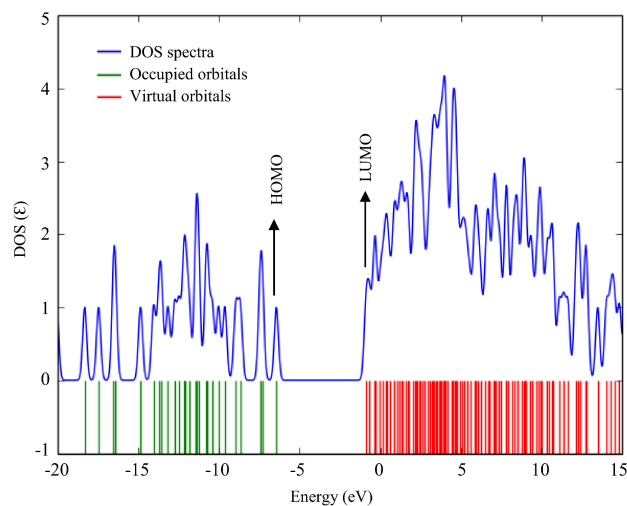
FIGURE 4. DOS spectrum of NAM using B3LYP/6-311++G(d,p) level in the range of -20 to 15 eV.

positive and negative phases, respectively. In the NAM, the HOMO represents the charge density localized over the side chain ($-C_5H_2SC_6H_3C_7H_2$) unit attached to a C3 atom; by contrast, the LUMO is located over the carboxyl group unit.

In order to obtain the total density of the state (DOS) curve of NAM as shown in Fig. 4, the output which extracts data from Gaussian .log file was analyzed and plotted as a graph using the Gauss Sum 3.0 program [49].

3.6. Electronic transitions

B3LYP/6-311++G(d,p) level using the TDDFT approach method on the previously optimized ground-state geometry of NAM was employed to simulate the optical properties of the molecule for the gas phase. The computed vertical excited singlet states, transition energies (E), wavelength (λ), and oscillator strengths (f) in the gas phase are tabulated in Table VII.

As it was clear from TDDFT/B3LYP calculation, the theoretical absorption bands in the UV region are correspond to two absorption maximum at $\lambda = 257.21$ with $E = 4.8204$ eV and $f = 0.0725$ and $\lambda = 384.61$ nm with $E = 3.2237$ eV and $f = 0.0092$ for gas phase at 6-311++G(d,p) basis set. Also, the maximum absorption wavelength corresponds to the electronic transition from the HOMO to LUMO with 100%. In the visible region, we found no calculated vertical transitions and seems to be with the same character as the experimental absorption spectra in this region. According to the experimental spectrum, the UV transparency cutoff occurs around 235 nm, and there is no absorption, and the crystal is colorless in the entire UV-Vis regions [27].

3.7. Molecular electrostatic potential

The electrostatic potential $V(\vec{r})$ at any point $\vec{r}$ for a molecular system having an electronic density function $\rho(\vec{r})$ is given by:

$$V(\vec{r}) = \sum_A \frac{Z_A}{|\vec{R}_A - \vec{r}|} - \int \frac{\rho(\vec{r}')d\vec{r}'}{|\vec{r}' - \vec{r}|}, \qquad (15)$$

TABLE VII. Absorption wavelengths (λ), excitation energies (E), oscillator strengths (f) and orbital configurations spectral transitions for NAM calculated at TDDFT (B3LYP/6-311++G(d,p)) (H=HOMO L=LUMO, H-2=HOMO-2, etc).

Excited States	Transition Character	Contribution	Spin Multiplicity	Symmetry	E (eV)	λ(nm)	f
S_1	H → L	100%	Singlet	A	2.2552	549.76	0.0005
S_2	H-4 → L	8%	Singlet	A	3.2237	384.61	0.0092
	H-2 → L	66%					
	H-1 → L	25%					
S_3	H-4 → L	4%	Singlet	A	3.3471	370.43	0.0002
	H-2 → L	21%					
	H-1 → L	75%					
S_4	H-4 → L	76%	Singlet	A	4.1504	298.73	0.0014
	H-3 → L	11%					
	H-2 → L	12%					
S_5	H-3 → L	2%	Singlet	A	4.7631	260.3	0.0015
	H → L+1	72%					
	H → L+3	21%					
	H → L+4	3%					
S_6	H-4→ L	10%	Singlet	A	4.8204	257.21	0.0725
	H-3 → L	86%					

-6.707e^{-2} [color bar] 6.707e^{-2}
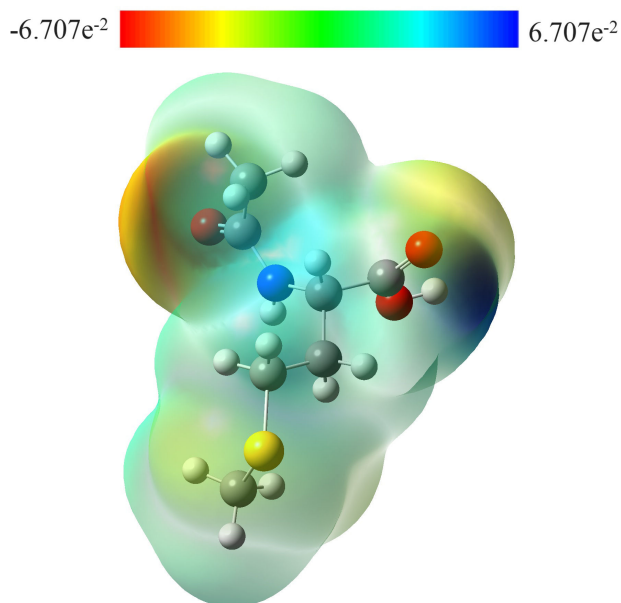
FIGURE 5. MEP surface of NAM using B3LYP/6-311++G(d,p) level of theory.

in which Z_A is the charge on nucleus A, located at $\vec{R}_A$. In this expression, the two terms represent the nuclear and electronic contributions to the potential, respectively.

The electrostatic potential is a physical observable, which can be determined experimentally by diffraction methods (50) and computationally. The Gaussian program calculates the potential at the points that located on the molecule's size on the $\rho(\vec{r})$ isodensity surface and then according to potential assigns colors to these points. In this way, MEP surface maps are surveyed. As is well known, MEP surfaces are useful diagrams that illustrate the charge distributions of molecules three-dimensionally. These maps allow us to visualize the charge distributions, charge related properties, size, and shape of molecules. Moreover, MEP provides interpreting and predicting relative reactivities sites for the electrophilic and nucleophilic attack, studies of the biological recognition process, hydrogen bonding interactions, molecular cluster, and crystal behavior, and the correlation and prediction of a wide range of macroscopic properties [51-55].

Figure 5 presents the MEP surface of the molecule under investigation is composed by using B3LYP/6-311++G(d,p) level of theory and a value of 0.0004 a.u. for the isodensity surface. On the map, the most negative (the lowest) and pos-

itive (the highest) electrostatic potentials are colored red and blue, respectively, and intermediate potentials are colored intermediate color spectrum.

Furthermore, the MEP map provides a visual method to understand the relationship between the structure and activity of the molecule. It is used to identify electrophilic and nucleophilic sites of a molecule. It can be seen from Fig. 5, the obtained electrostatic potential is composed of the positive electrostatic potential around the O1 atom in the peptide group, which is the most reactive site for nucleophilic attack. The negative electrostatic potential is mainly localized around the N-H in the peptide group region and O3-H in the carboxyl group, which is the possible site for electrophilic attack. The remaining green areas of the molecule (C-C bonds) are surrounded by close to zero electrostatic potential.

4. Conclusions

This study analyzes computational studies on N-acetyl-DL-methionine. We have calculated the geometric parameters, vibrational frequencies, ^{13}C and ^{1}H NMR values, the nonlinear optical properties, frontier molecular orbitals, UV-Vis calculations, and molecular electrostatic potential surface of the monomer form of the N-acetyl-DL-methionine using DFT methods with 6-311++G(d,p) basis set. In particular, a good agreement between experimental and calculated vibrational frequencies has been observed. DFT/HSEH1PBE method has shown a better fit to experimental ones than DFT/B3LYP in evaluating vibrational frequencies. The nonlinear optical behavior of the title molecule was investigated by the determination of the dipole moment, the polarizability, and the first-order hyperpolarizability. The HOMO-LUMO energy gap results reveal that the NAM is the highest kinetic stability and can be termed as a hard molecule with the largest HOMO-LUMO gap of average 5.319 eV. The molecular electrostatic potential surface has also been drawn to explain the activity of the title molecule. In general, we can easily state that the theoretical results obtained from our studies for the mentioned compound are in good agreement with the experimental data. Hence, we anticipate that the present quantum chemical study will be very useful in the understanding of the structure, activity, and dynamics of the molecule. We hope that our results for N-acetyl-DL-methionine would provide more information for further investigation in the future.

1. T. Willke, Methionine production-a critical review, *Appl. Microbiol. Biotechnol.* **98** (2014) 9893, https://doi.org/10.1007/s00253-014-6156-y.

2. M. J. Frisch, H. P. Hratchian, and A. B. Nielsen, *Gaussian 09: Programmer's Reference*, (Gaussian, 2009).

3. R. Dennington, T. Keith, and J. Millam, *GaussView, Version 5*, (Semichem Inc., Shawnee Mission, KS, 2009).

4. A. D. Becke, Density-functional exchange-energy approximation with correct asymptotic behavior, *Phys. Rev. A* **38** (1988) 3098, https://doi.org/10.1103/PhysRevA.38.3098.

5. A. D. Becke, Density functional thermochemistry. IV. A new dynamical correlation functional and implications for exact exchange mixing, *J. Chem. Phys.* **104** (1996) 1040, https://doi.org/10.1063/1.470829.

6. C. Lee, W. Yang, and R. G. Parr, Development of the Colle-Salvetti correlation-energy formula into a functional of the electron density, *Phys. Rev. B* **37** (1988) 785, https://doi.org/10.1103/PhysRevB.37.785.

7. J. Heyd, G. E. Scuseria, and M. Ernzerhof, Hybrid functionals based on a screened Coulomb potential, *J. Chem. Phys.* **118** (2003) 8207, https://doi.org/10.1063/1.1564060.

8. J. Heyd and G. E. Scuseria, Assessment and validation of a screened Coulomb hybrid density functional, *J. Chem. Phys.* **120** (2004) 7274, https://doi.org/10.1063/1.1668634.

9. J. P. Perdew, K. Burke, and M. Ernzerhof, Generalized gradient approximation made simple, *Phys. Rev. Lett.* **77** (1996) 3865, https://doi.org/10.1103/physrevlett.77.3865.

10. M. E. Ochoa, P. Labra-Vázquez, N. Farfán, and R. Santillan, Designed synthesis and crystallization of isomorphic molecular gyroscopes with cell-like bilayer self-assemblies, *Cryst. Growth Des.* **18** (2018) 2795, https://doi.org/10.1021/acs.cgd.7b01542.

11. F. London, Théorie quantique des courants interatomiques dans les combinaisons aromatiques, *J. Phys. Radium* **8** (1937) 397, https://doi.org/10.1051/jphysrad:01937008010039700.

12. R. McWeeny, Perturbation theory for the Fock-Dirac density matrix, *Phys. Rev.* **126** (1962) 1028, https://doi.org/10.1103/PhysRev.126.1028.

13. R. Ditchfield, Self-consistent perturbation theory of diamagnetism: I. A gauge-invariant LCAO method for N.M.R. chemical shifts, *Mol. Phys.* **27** (1974) 789, https://doi.org/10.1080/00268977400100711.

14. K. Wolinski, J. F. Hinton, and P. Pulay, Efficient implementation of the gauge-independent atomic orbital method for NMR chemical shift calculations, *J. Am. Chem. Soc.* **112** (1990) 8251, https://doi.org/10.1021/ja00179a005.

15. J. R. Cheeseman, G. W. Trucks, T. A. Keith, and M. J. Frisch, A comparison of models for calculating nuclear magnetic resonance shielding tensors, *J. Chem. Phys.* **104** (1996) 5497, https://doi.org/10.1063/1.471789.

16. T. A. Keith and R. F. W. Bader, Calculation of magnetic response properties using atoms in molecules, *Chem. Phys. Lett.* **194** (1992) 1, https://doi.org/10.1016/0009-2614(92)85733-Q.

17. T. A. Keith and R. F. W. Bader, Calculation of magnetic response properties using a continuous set of gauge transformations, *Chem. Phys. Lett.* **210** (1993) 223, https://doi.org/10.1016/0009-2614(93)89127-4.

18. P. Labra-Vázquez, A. Z. Lugo-Aranda, M. Maldonado-Domínguez, R. Arcos-Ramos, M. Carreón-Castro, R. Santillán, and N. Farfán, On the molecular structure of (E)-3-(9H-fluoren-2-yl)-1-(pyridin-2-yl) prop-2-en-1-one, theoretical calculations and SXRD studies, *J. Mol. Struct.* **1101** (2015) 116, https://doi.org/10.1016/j.molstruc.2015.08.023.

19. T. Pawlak, D. Czajkowska-Szczykowska, I. Jastrzebska, R. Santillan, B. Seroka, J. Maj, J. W. Morzycki, P. Labra-Vázquez, N. Farfán, G. D. Bujacz, and M. J. Potrzebowski, Influence of Hydrogen/Fluorine Substitution on Structure, Thermal Phase Transitions, and Internal Molecular Motion of Aromatic Residues in the Crystal Lattice of Steroidal Rotors, *Cryst. Growth Des.* **20** (2020) 2202, https://doi.org/10.1021/acs.cgd.9b01179.

20. E. Runge and E. K. U. Gross, Density-functional theory for time-dependent systems, *Phys. Rev. Lett.* **52** (1984) 997, https://doi.org/10.1103/PhysRevLett.52.997.

21. R. Bauernschmitt and R. Ahlrichs, Treatment of electronic excitations within the adiabatic approximation of time dependent density functional theory, *Chem. Phys. Lett.* **256** (1996) 454, https://doi.org/10.1016/0009-2614(96)00440-X.

22. E. K. U. Gross, J. F. Dobson, and M. Petersilka, *Density Functional Theory II: Relativistic and Time Dependent Extensions*, edited by R. F. Nalewajski (Springer, Berlin, Heidelberg, 1996), pp. 81-172, https://doi.org/10.1007/BFb0016643.

23. K. Burke and E. K. U. Gross, *Density Functionals: Theory and Applications*, edited by D. Joubert (Springer, Berlin, Heidelberg, 1998), pp. 116-146, https://doi.org/10.1007/BFb0106735.

24. M. E. Casida, C. Jamorski, K. C. Casida, and D. R. Salahub, Molecular excitation energies to high-lying bound states from time-dependent density-functional response theory: Characterization and correction of the time-dependent local density approximation ionization threshold, *J. Chem. Phys.* **108** (1998) 4439, https://doi.org/10.1063/1.475855.

25. M. N. Ponnuswamy and J. Trotter, N-Acetyl-DL-methionine, C7H13NO3S, *Acta Cryst. C* **41** (1985) 917, https://doi.org/10.1107/S0108270185005996.

26. E. E. Kim, A. Sicignano, and K. Eriks, Binding of calcium to amino acids: the crystal structure of pentaaquobis(hydroxy-(L)-prolinato)calcium, $Ca(C_5H_8O_3N)_{2.5}H_2O$, *J. Am. Chem. Soc.* **107** (1985) 6042, https://doi.org/10.1021/ja00307a036.

27. K. Moovendaran and S. Natarajan, Growth of bulk single crystal of N-acetyl DL-methionine and its spectral characterization, *Spectrochim. Acta A* **135** (2015) 317, https://doi.org/10.1016/j.saa.2014.07.012.

28. W. He, G. Zhou, J. Li, and A. Tian, Molecular design of analogues of 2,6-diamino-3,5-dinitropyrazine-1-oxide, *J. Mol. Struct.* **668** (2004) 201, https://doi.org/10.1016/j.theochem.2003.10.058.

29. N. Dege, N. Şenyüz, H. Bat?, N. Günay, D. Avc?, Ö. Tamer, and Y. Atalay, The synthesis, characterization and theoretical study on nicotinic acid [1-(2,3-dihydroxyphenyl)methylidene]hydrazide, *Spectrochim. Acta A* **120** (2014) 323, https://doi.org/10.1016/j.saa.2013.10.030.

30. B. G. Johnson, P. M. W. Gill, and J. A. Pople, The performance of a family of density functional methods, *J. Chem. Phys.* **98** (1993) 5612, https://doi.org/10.1063/1.464906.

31. A. P. Scott and L. Radom, Harmonic vibrational frequencies: an evaluation of Hartree-Fock, Møller-Plesset, quadratic configuration interaction, density functional theory, and semiempirical scale factors, *J. Phys. Chem.* **100** (1996) 16502, `https://doi.org/10.1021/jp960976r`.

32. H. Pir, N. Günay, D. Avcı, and Y. Atalay, Molecular structure, vibrational spectra, NLO and NBO analysis of bis(8-oxy-1-methylquinolinium)hydroiodide, *Spectrochim. Acta A* **96** (2012) 916, `https://doi.org/10.1016/j.saa.2012.07.044`.

33. C. R. Zhang, H. S. Chen, and, G. H. Wang, Structure and properties of semiconductor microclusters GanPn(n=1-4): A first principle study, *Chem. Res. Chin. Univ.* **20** (2004) 640.

34. Y. Sun, X. Chen, L. Sun, X. Guo, and W. Lu, Nanoring structure and optical properties of Ga8As8, *Chem. Phys. Lett.* **381** (2003) 397, `https://doi.org/10.1016/j.cplett.2003.09.115`.

35. O. Christiansen, J. Gauss, and J. F. Stanton, Frequency-dependent polarizabilities and first hyperpolarizabilities of CO and H2O from coupled cluster calculations, *Chem. Phys. Lett.* **305** (1999) 147, `https://doi.org/10.1016/S0009-2614(99)00358-9`.

36. D. A. Kleinman, Nonlinear dielectric polarization in optical media, *Phys. Rev.* **126** (1962) 1977, `https://doi.org/10.1103/PhysRev.126.1977`.

37. D. A. Dixon and N. Matsuzawa, Density functional study of the structures and nonlinear optical properties of urea, *J. Phys. Chem.* **98** (1994) 3967, `https://doi.org/10.1021/j100066a011`.

38. A. J. Garza, G. E. Scuseria, S. B. Khan, and A. M. Asiri, Assessment of long-range corrected functionals for the prediction of non-linear optical properties of organic materials, *Chem. Phys. Lett.* **575** (2013) 122, `https://doi.org/10.1016/j.cplett.2013.04.081`.

39. L. T. Cheng, W. Tam, S. H. Stevenson, G. R. Meredith, G. Rikken, and S. R. Marder, Experimental investigations of organic molecular nonlinear optical polarizabilities. 1. Methods and results on benzene and stilbene derivatives, *J. Phys. Chem.* **95** (1991) 10631, `https://doi.org/10.1021/j100179a026`.

40. W. D. Kumler and G. M. Fohlen, The Dipole Moment and Structure of Urea and Thiourea1, *J. Am. Chem. Soc.* **64** (1942) 1944, `https://doi.org/10.1021/ja01260a054`.

41. C. C. Teng and A. F. Garito, Dispersion of the nonlinear second-order optical susceptibility of organic systems, *Phys. Rev. B* **28** (1983) 6766, `https://doi.org/10.1103/PhysRevB.28.6766`.

42. M. Stähelin, D. M. Burland, and J. E. Rice, Solvent dependence of the second order hyperpolarizability in p-nitroaniline, *Chem. Phys. Lett.* **191** (1992) 245, `https://doi.org/10.1016/0009-2614(92)85295-L`.

43. R. W. Godby, M. Schlüter, and L. J. Sham, Self-energy operators and exchange-correlation potentials in semiconductors, *Phys. Rev. B* **37** (1988) 10159, `https://doi.org/10.1103/PhysRevB.37.10159`.

44. T. Koopmans, Über die Zuordnung von Wellenfunktionen und Eigenwerten zu den einzelnen Elektronen eines Atoms, *Physica* **1** (1934) 104, `https://doi.org/10.1016/S0031-8914(34)90011-2`.

45. R. S. Mulliken, A new electroaffinity scale; together with data on valence states and on valence ionization potentials and electron affinities, *J. Chem. Phys.* **2** (1934) 782, `https://doi.org/10.1063/1.1749394`.

46. R. G. Pearson, Hard and soft acids and bases, *J. Am. Chem. Soc.* **85** (1963) 3533, `https://doi.org/10.1021/ja00905a001`.

47. R. G. Pearson, Hard and soft acids and bases, HSAB, part 1: Fundamental principles, *J. Chem. Educ.* **45** (1968) 581, `https://doi.org/10.1021/ed045p581`.

48. R. G. Pearson, Maximum chemical and physical hardness, *J. Chem. Educ.* **76** (1999) 267, `https://doi.org/10.1021/ed076p267`.

49. N. M. O'Boyle, A. L. Tenderholt, and K. M. Langner, cclib: A library for package-independent computational chemistry algorithms, *J. Comput. Chem.* **29** (2008) 839, `https://doi.org/10.1002/jcc.20823`.

50. P. Politzer and D. G. Truhlar, *Chemical applications of atomic and molecular electrostatic potentials: reactivity, structure, scattering, and energetics of organic, inorganic, and biological systems* (Springer, New York, 2013), pp. 1-6, `https://doi.org/10.1007/978-1-4757-9634-6`.

51. E. Scrocco and J. Tomasi, *New concepts II*, edited by A. Davison and M. J. S. Dewar (Springer, Berlin, Heidelberg, 1973), pp. 95-170, `https://dx.doi.org/10.1007/3-540-06399-4_6`.

52. E. Scrocco and J. Tomasi, *Advances in quantum chemistry, edited by P. Löwdin* (Acedemic Press, New York, 1978), pp.115-193, `https://doi.org/10.1016/S0065-3276(08)60236-1`.

53. P. Politzer and K. C. Daiker, *The force concept in chemistry*, edited by B. M. Deb (Van Nostrand Reinhold, New York, 1981), pp. 294-387.

54. P. Politzer, P. R. Laurence, and K. Jayasuriya, *Molecular electrostatic potentials: An effective tool for the elucidation of biochemical phenomena,* Environ. Health Perspect. **61** (1985) 191, `https://doi.org/10.1289/ehp.8561191`.

55. P. Politzer and J. S. Murray, The fundamental nature and role of the electrostatic potential in atoms and molecules, *Theor. Chem. Acc.* **108** (2002) 134, `https://doi.org/10.1007/s00214-002-0363-9`.